Research article

# Solid-phase transient soldering method based on Au/Ni–W multilayer thin-film-modified copper-based structures

Jin Xiao [a,b,*], Qian Zhai [a], Jia Luo [b]

[a] School of Mechanical and Electrical Engineering, Guangzhou Huali College, Guangzhou 511300, China
[b] School of Intelligent Manufacturing and Materials Engineering, Gannan University of science and technology, Ganzhou 341000, China

A B S T R A C T

The copper crystal cone-shaped micro-nanostructure is used as the substrate, and the Ni–W alloy layer and Au nanolayer are plated sequentially. Instantaneous soldering with lead-free solder is realized under ultrasonic assistance at room temperature. This solves the residual stress and thermal damage caused by high melting point lead-free solder on thin chips and thermal components, and ensures the safety and reliability of electronic components. Copper-based microstructures are deposited by electrochemical methods. An amorphous Ni–W alloy layer with a thickness of 180 nm is deposited on the Cu-based microstructures by adjusting the atomic ratio of the plating solution. The Ni–W layer is further coated with a 50 nm Au layer to prevent oxidation. Solid-phase transient soldering is realized by combining the Au/Ni–W multilayer thin-film-modified Cu substructures with commercial solder (SAC305) for a holding time of 3 s at a soldering pressure of 10,000 gf (20 MPa) while ultrasonically assisted. The soldered samples are aged at 180 °C for 10 min, 30 min, and 60 min, respectively. Copper substructures with different surface modifications are subjected to destructive shear experiments with solder balls. Scanning electron microscope and X-ray fluorescence thickness gauge are used to study the microstructure, intermetallic compound (IMC) composition thickness and properties of the soldered interface and section. The cone height of the Cu-based structure is 2–4 μm, and the diameter of the bottom is 800 nm–1200 nm, which has a sharp tip and an excellent L/D ratio. The interface between the Au/Ni–W modified Cu substructure and the solder ball is almost free of holes. The average shear strength at the soldering interface is about 43.06 MPa. The fracture surface after the shear experiment basically occurs inside the solder ball matrix, which belongs to the pure toughness fracture. The interface between the Au/Ni–W-modified Cu-based structure and the solder ball is subjected to long aging treatment at 180 °C. The soldering interface showed a "bright layer". New phases are generated on the solder side above the "bright layer", while no new phases appear on the Cu substructure side below the "bright layer". The copper-based microstructure is inserted into the inside of the solder ball to form an inlay and produce mechanical interlocking. Au/Ni–W alloy modification layer can effectively improve the surface hardness of copper-based structures. This creates a large hardness difference with soft solder and enables the formation of fewer holes in the insertion solder. Amorphous Ni–W alloys are prone to form dense oxide films during ultrasonication. The Au film modification prevents oxide generation and increases the average shear strength of the soldering interface. The Ni–W alloy layer retards the interdiffusion between

---

* Corresponding author. No. 11 Huali Rd., Zengcheng District, Guangzhou Huali College, Guangzhou 511300, China.
   *E-mail address:* 67104869@qq.com (J. Xiao).

Cu–Sn, blocks the excessive growth of Cu–Sn IMCs, and reduces the reliability problems caused by interface failure.

## 1. Introduction

People have a higher pursuit of miniaturization and refinement of electronic products. However, the feature size of the chip is close to the manufacturing limit, and high-density three-dimensional stacked packaging technology is the inevitable trend of electronic packaging technology development [1–5]. There are more chips stack in the future development trend. Chips and modules are becoming ever smaller in thickness. Solder junctions will get smaller and smaller in size. Soldering technology is the key to realize vertical interconnection [6–10]. Among the various soldering techniques, metal-to-metal soldering provides both good mechanical support and electrical interconnections. Common metal-to-metal soldering combinations include Cu–Cu, Au–Au, Au–In, Au–Sn, Pb–Sn, and Cu–Sn [11–16]. However, Cu–Cu soldering requires extremely low surface roughness, ultra-high pressure, and harsh vacuum environments [17,18]. Although Au and In are expensive and rare metals, Au–In intermetallic compounds can be formed at lower temperatures (160 °C) and can be used for low-temperature solder bonding [19–21]. Sn–Pb eutectic is a well-established low-temperature soldering method. However, the use of traditional Sn–Pb solder is limited due to environmental pollution and poor thermal workability. Lead-free solder will gradually replace Sn–Pb solder in the electronics industry [22,23]. Lead-free Cu–Sn solder is widely used for vertical stacking in 3D interconnects due to its low cost and high process compatibility [24,25]. However, lead-free solder has a high melting point. The melting point of Sn–3Ag-0.5Cu (SAC305), a commercial solder, is 230 °C, almost 40 °C higher compared with the 183 °C melting point of Sn–37Pb solder. The high temperature causes high thermal damage to thin chips and thermally sensitive devices, leading to wafer warpage and thermal stress, and degradation of device performance [26,27]. Collapse and spillage of solder in molten soldering is inevitable. Tin spillage may lead to short circuits. Interconnect density is limited. As the size and pitch of solder joints become smaller and smaller, residual flux removal is difficult, which adversely affects the device performance in use. Moreover, high temperature conditions will accelerate the diffusion of atoms at the solder interface, forming Kirkendall holes and threatening device reliability [28–30]. Cu–Sn low-temperature solid-state soldering has been considered as a potential solution to the above problems, where the soldering temperature ranges from 150 °C to 220 °C [31,32]. Wang [33] et al. investigated a low-temperature soldering technique using graphene as an interlayer. During the soldering process, dependable Sn–Cu junctions were achieved at a temperature of 150 °C by incorporating nanoscale graphene/copper composites onto a copper substrate. The single graphene interlayer, which is mechanically strong and extremely conductive, can effectively impede the formation of IMCs. It can effectively stop aging problems. However, the synthesis and transfer process of graphene is complicated. Li [34] et al. doped SiC nanowires into tin solder to obtain transient liquid phase soldering at 250 °C. The sandwich Cu/Sn-0.6SiC/Cu joints obtained had excellent shear strength. The fracture surface was along-crystal fracture. SiC nanowires dispersed in the tin solder hinder the growth path between Sn and Cu. This results in slowing down the growth of IMCs. Sun [35] et al. used electrochemical methods to obtain Cu–Co–P microcone structures up to 5 μm with sharp top corners. They were pressed together with tin-based solder at 170 °C. However, the filling of the solder at the root of the microcones and the closing of the holes required higher temperatures or increased pressure, which is contrary to the original purpose of low-temperature soldering. Optimizing the morphology of the microcones in terms of height, base diameter, top angle, and density may be a potential way to achieve seamless soldering at low temperatures and pressures.

In this paper, a copper-based microstructure with special morphology is used as the basis. An amorphous Ni–W alloy layer with a thickness of 180 nm and an Au modification layer with a thickness of 5 nm were sequentially coated on it. Solid-phase transient soldering of this Ni–W multilayer thin-film-modified Cu-based microstructure with a Sn-based solder (SAC305) was realized under the soldering pressure of 10,000 gf (20 MPa) for 3 s and the simultaneous assisted ultrasonic vibration condition. The Cu-based microstructures were inserted inside the solder balls to form inlays, producing mechanical interlocking. The Au/Ni–W alloy modification
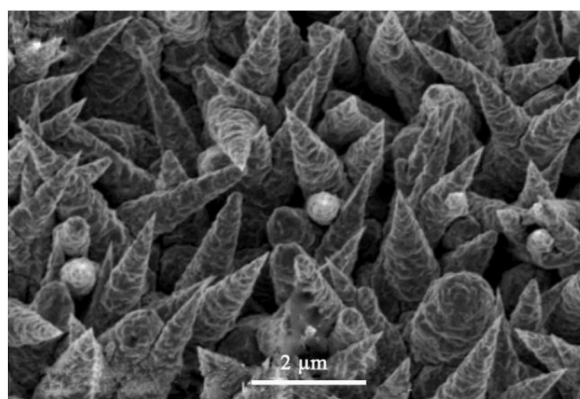


**Fig. 1.** SEM image of Cu-based micro-nano hierarchical structures.

layer can effectively improve the surface hardness of copper-based microstructures. This forms a large hardness difference with the tin solder, reducing the formation of holes in the insertion soldering and providing excellent soldering results. The soldering interface has an average shear strength of up to 43.06 MPa. High-density three-dimensional packaging technology is anticipated to use this solid-phase transient soldering technology.

## 2. Experiment

The Ni–W multilayer thin film modified Cu-based microstructures selected in this paper have a three-layer structure. The first layer structure is the Cu-based micro-nano hierarchical structure prepared by chemical plating. The plating solution was formulated as the main salt $CuSO_4 \cdot 5H_2O$ (10 g/L), $NiSO_4 \cdot 5H_2O$ (1 g/L), buffer $H_3BO_3$ (20 g/L), reducing agent $Na_3C_6H_5O_7$ (20 g/L), $NaH_2PO_2$ (25 g/L), crystallization adjuster PEG (2 g/L), and NaOH (8 g/L). The plating solution temperature was 60 °C. The morphology was specially controlled, requiring the copper protrusion structure to be morphologically complete with good vertical directionality and height consistency. The type and content of the crystallization modifier, as well as the deposition time, may be used to control morphology and size of protrusion structures. The height of the copper-based micrometer-scale protrusions is in the range of 2–4 μm. The protrusion structures require to have a sharp tip and a wide base size of 800 nm–1200 nm. The density and aspect ratio of the protrusion structures are excellent, as shown in Fig. 1. The formation of these unique structures is attributed to the role of PEG in controlling the growth rate of different copper crystalline surfaces. The use of PEG as a single additive is based on the concept of inhomogeneous distribution of adsorption. PEG with higher molecular weight has better inhibition of nucleation and crystal growth (especially root diameter) by adsorption and desorption, thus controlling the growth rate of these crystal facets. The second structure was a Ni–W alloy layer, obtained by electrodeposition on a copper-based micro- and nano-graded structure. The electroplating solution was based on nickel chloride and sodium tungstate as the main salts and citric acid as the complexing agent. The amorphous Ni–W alloy was obtained by adjusting the ratio of W and Ni atoms in the plating solution. The composition of the alloy plating solution was $Na_3C_6H_5O_7 \cdot 2H_2O$ (75 g/L), HEDP (50 wt%) (45 g/L), $Na_2WO_4 \cdot 2H_2O$ (65 g/L), $NiCl_2 \cdot 6H_2O$ (25 g/L), pH 5.0–6.0, plating solution temperature 65 °C, and current density (4 A/dm$^2$). The plating time was 180 s, and the thickness of the plated layer was about 180 nm. As shown in Fig. 2, the copper-based micro-nano hierarchical surface structure has obvious fine raised structures. This is the Ni–W alloy small particles. However, the morphology of the Cu-based micro-nano-graded structure is well preserved, and it is still in the shape of a round needle cone. The third structure is the Au modification layer. Since the Ni–W layer is easily oxidized, an Au layer was electrodeposited on it to prevent oxidation. The Au layer was plated using a pulsed DC power supply with a pulse frequency of 100 Hz, a duty cycle of 1:9, a current density of 0.3 A/dm$^2$, a plating solution temperature of 50 °C, and a pH value of 5.0–6.0. The composition of the plating solution was $KAu(CN)_2$ (0.6 g/L). The plating time was 20 s. The thickness of the plated layer was about 5 nm. As shown in Fig. 3, the surface of the plated Au layer was relatively flat and smooth. The Au layer was uniformly covered on the surface of the Cu-based microstructure without small bumps, and the adhesion of the Au layer to the substrate was good without delamination.

A lead-free solder ball (Sn-3.0Ag-0.5Cu, SAC305) was selected as one end of the soldering couple with a diameter of 650 μm. The solder ball was cleaned in a 10 % $H_2SO4$ solution (10 % by volume) for 20 s, rinsed with anhydrous ethanol and ultrapure water in turn, blown dry and set aside. The study utilized a specialized ultrasonic micro solder joint soldering system (Rhesca PTR-1102). The fixed frequency of the ultrasonic system was configured at 15 KHz, while the loading parameters such as pressure and time were accurately regulated through computer control. Fig. 4(a) shows the soldering schematic. The detailed instructions are outlined below: firstly, the C194 copper substrate coated with Au/Ni–W/Cu multilayer film is placed on the carrier base plate of the soldering instrument, and the solder ball is placed on top of the C194 copper substrate. The position of the soldering ball can be adjusted by moving the carrier base plate by shaking the handle, so that the tip of the soldering ball and the center of the indenter is aligned. The height of the indenter is slowly adjusted. The indenter stops at a distance of about 1 mm above the solder ball. The speed at which the indenter descends has been adjusted to 0.05 mm/s. The pressure is preset to 10,000 gf and the holding time for loading is preset to 3 s. Then the soldering program is switched on. When the indenter comes into contact with the solder ball, the vertical load is applied and the ultrasonic
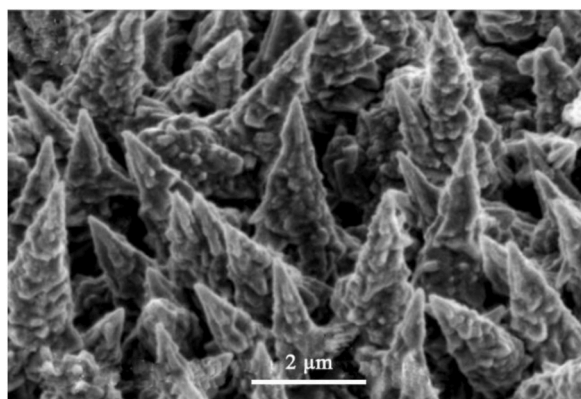


**Fig. 2.** SEM image of surface-modified Ni–W alloy Cu-based micro-nano hierarchical structures.
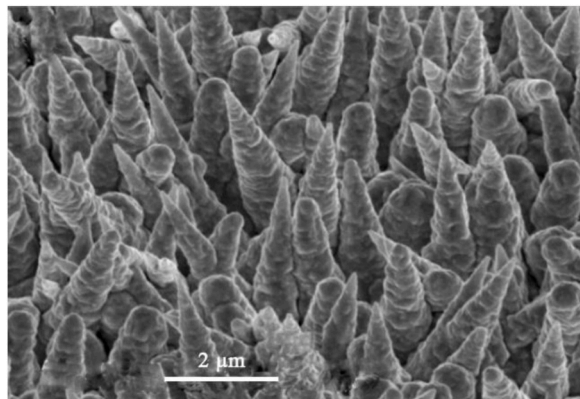
**Fig. 3.** SEM image of surface-modified Au/Ni–W Cu-based micro-nano hierarchical structures.
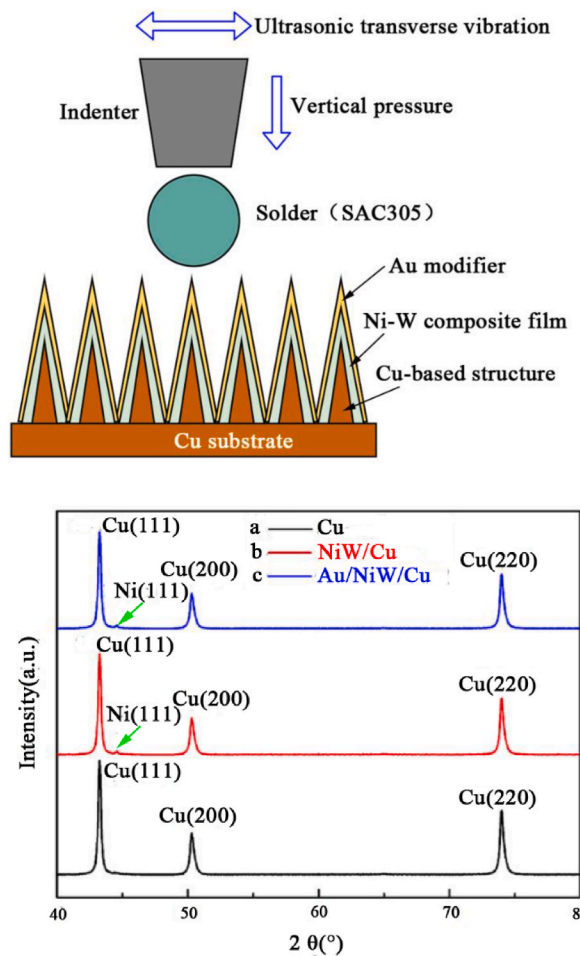


**Fig. 4.** The soldering process:(a) Schematic diagram (b) XRD spectra of Cu micro-nanolayers with different modification layers.

transverse vibration is started at the same time. When the pressure reaches the preset value, the sensor feeds back and starts calculating the loading time. When the loading time reaches the preset value, the indenter lifts and returns to its original position. Fig. 4(b) shows the X-ray diffraction patterns before and after the modification of the Cu micro- and nanolayers. a line is the pattern of Cu micro- and nanolayers. b line is the pattern of Cu micro- and nanolayers modified by the Ni–W alloy. c line is the pattern of Cu micro- and nanolayers modified by the Au/Ni–W layer. As can be seen from lines a, b, and c, the three strong diffraction peaks are at 43°, 51°, and

74°, which correspond to the (111), (200), and (220) crystal planes of Cu, respectively. According to the PDF#04–0836 card, the element can be identified as Cu. b and c lines have weaker diffraction peaks present at 44°, corresponding to the (111) crystal plane of Ni. According to the PDF#04–0850 card, this element can be identified as Ni. Since the Au modification layer is only about 5 nm, its content is very small, and no diffraction peaks are detected.

The shear damage mode of the soldering instrument was selected to test the average shear strength of interface between the copper-based microstructures and the solder ball. Nine measurements were taken for each sample and averaged to minimize measurement error.
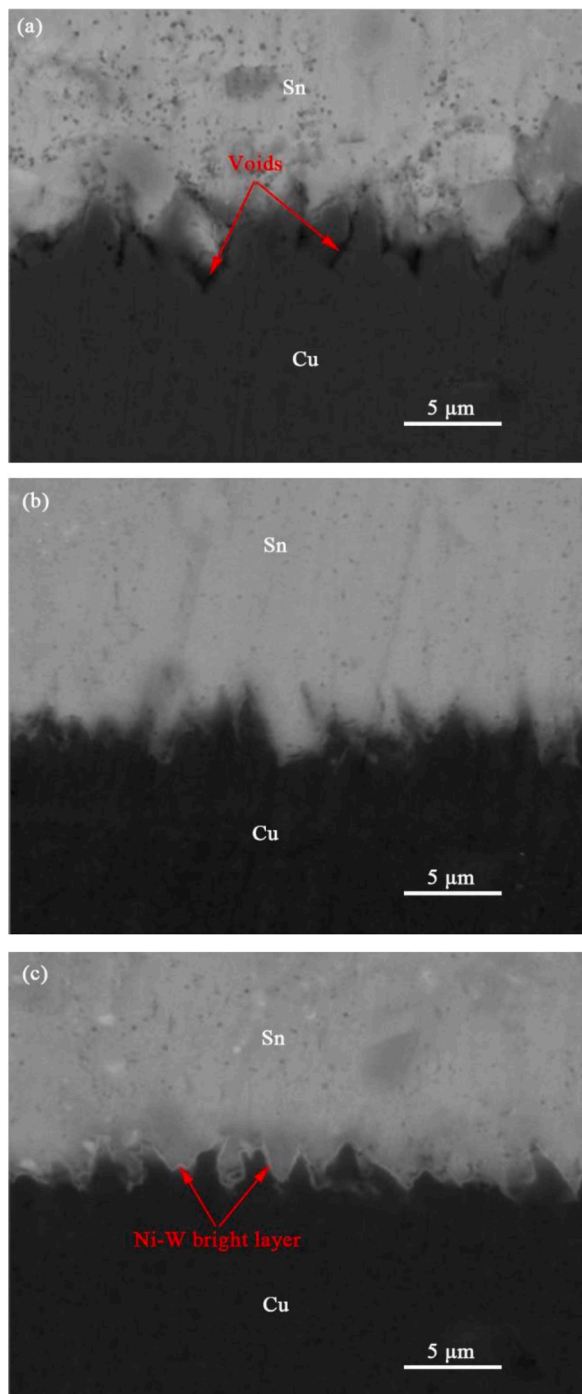


**Fig. 5.** Microstructure of SAC305 soldering interface with different Cu-based micro-nanostructures: (a) Pure Cu-based micro-nanostructures (b) Ni–W alloy modified Cu-based micro-nanostructures (c) Au/Ni–W modified Cu-based micro-nanostructures.

Field emission scanning electron microscope (Hitachi Regulus 8100) was used to observe the morphology of the soldering interface, the morphology of the fracture surface, and quantitatively analyze the tissue composition and element distribution at the soldering interface. X-ray fluorescence thickness meter (Hitachi X strata 920) was used to measure the thickness of copper-based microstructure modification layer. Different positions were selected for multiple measurements to obtain the average value.

## 3. Results and discussion

### 3.1. Soldering interface microstructure

Fig. 5(a) shows the interface between the pure copper-based micro-nano-graded structure and the solder ball soldered at a soldering pressure of 10,000 gf (20 MPa), a soldering time of 3 s, and ultrasonic vibration of 3 s. The upper part with lighter color was tin-based solder. The darker color of the lower part was the copper-based micro-nano-graded structure. It was found that the copper-based micro-nano-graded structure can be fully embedded inside the solder, but there were still holes present in the lower cavity of the micro-nano-structure located at the solder interface. Fig. 5(b) shows the soldering interface between the Ni–W alloy layer-modified Cu-based structure with a thickness of 180 nm and the solder ball at a soldering pressure of 10,000 gf (20 MPa), a soldering time of 3 s, and ultrasonic vibration of 3 s. It was found that the Ni–W alloy layer-modified Cu-based structure with a thickness of 180 nm can fully embed into the solder, but there were still holes at the bottom concave of the micro-nanostructure at the solder interface. The interface quality between the Cu substructure, which was coated with a 180 nm Ni–W alloy layer, and the SAC305 solder ball exhibited satisfactory performance. The degree of embedding of the micro-nanostructures was sufficient. There were almost no holes in the solder joints. There was obvious diffusion at the solder interface. Fig. 5(c) shows the soldering interface between the Ni–W alloy layer with a thickness of 180 nm and the 5 nm Au film-modified Cu-based microstructure and the solder ball with a soldering pressure of 10,000 gf (20 MPa), a soldering time of 3 s, and ultrasonic vibration for 3 s. It was found that the soldering interface between the Au/Ni–W modified Cu-based microstructure and the SAC305 solder ball exhibited a good mechanical embedding effect. No holes were found at the bottom recess of the microstructures. A layer of Ni–W alloy modification was found above the Cu-based structure at the solder interface, which has a distinctive lining and is a "bright layer" structure. It shows a clear demarcation line between the soft brazing layer and the copper-based micro- and nano-graded structure. Since the Ni–W alloy layer has a higher hardness than the pure Cu-based microstructure, this further increases the hardness contrast with the soft brazing solder. Under constant soldering parameters, this harder structure can be more fully embedded inside the solder.

### 3.2. Average shear strength at the interface between solder and different copper substrates

Copper-based structures coated with different modification layers were subjected to destructive shear testing with SAC305 solder balls at a soldering pressure of 10,000 gf (20 MPa), a soldering time of 3 s, and ultrasonic vibration of 3 s. The shear results are shown in Fig. 6. The average shear strength between the Cu-based microstructure with Au/Ni–W surface modification layer and the solder ball is 43.2 MPa, which is comparable to the reflow soldering process. The pure Cu-based microstructure without any surface modification layer has the highest average shear strength of 45.8 MPa, while the Cu-based microstructure with a Ni–W surface modification layer has the smallest average shear strength of 23.4 MPa, which is attributed to the amorphous structure of Ni–W alloy obtained by adjusting the ratio of Ni and W atoms in the plating solution. This amorphous Ni–W layer forms an oxide film under high temperature conditions due to friction during the ultrasonic process. This dense oxide film is chemically stable and does not react with the atoms in the solder ball, blocking the copper structure from the tin-based solder and preventing the formation of an effective bond. Secondly, additional energy consumption is required for the copper structure to puncture this oxide film. Therefore the solder strength between the copper-based microstructure coated with Ni–W alloy and the solder ball is greatly reduced. After further coating of Au film on the surface of Ni–W alloy layer, the Au film can effectively prevent the oxidation problem of Ni–W layer. Moreover, the Au atoms have high
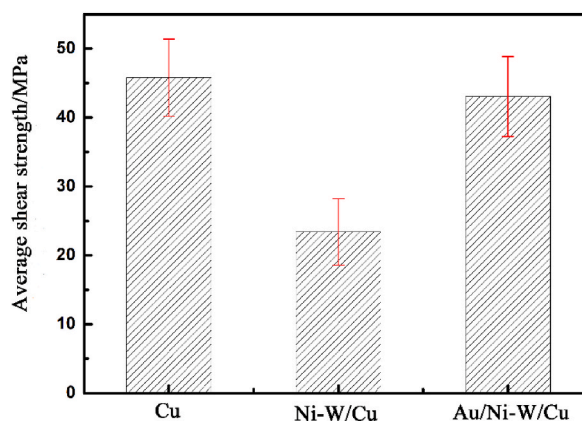


**Fig. 6.** Relationship between copper-based micro- and nano-hierarchical structures with different modification layers and average shear strength.

activation energy, which makes the Au film and the Sn atomic energy diffuse quickly to have solid solution reaction to obtain a stable interface and improve the average shear strength of the soldering interface.

### 3.3. Organization and morphology of the fracture surface at the soldering interface

During hot compression soldering, the bottom of the solder ball first comes into contact with the tip of the copper-based microstructure. Then the ball starts to collapse and spread out under vertical pressure and ultrasonic transverse vibration until the end of the hot compression soldering. The copper-based microstructures were inserted into the solder ball to form an inlay during the soldering process. Therefore, in the shear test, due to the binding effect of the solder interface, the solder ball caused the internal material of the solder to fracture during the rolling process. Part of the solder remains on the copper structure. The amount of solder remaining on the copper structure is proportional to the size of the bonding force of the solder couple. The fracture surfaces of copper-based
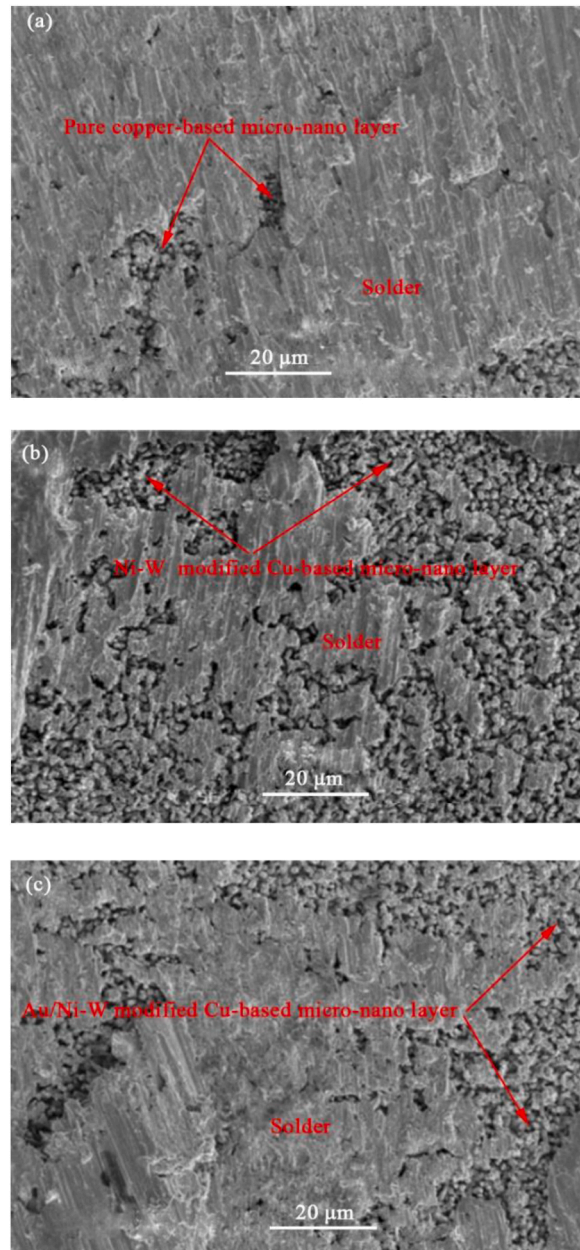


**Fig. 7.** Fracture surface morphology at the interface of different modification layers of copper-based micro- and nano-hierarchical structures with SAC305 soldering: (a) Pure Cu-based micro-nanostructures (b) Ni–W alloy modified Cu-based micro-nanostructures (c) Au/Ni–W modified Cu-based micro-nanostructures.

microstructures and solder balls with different modification layers damaged by shear force were observed. The residual solder was found to be more nearer to the center of the solder and less nearer to the edge places. It was found that different amounts of residual solder were distributed on the copper-based microstructure. And the amount of residual solder is related to the type of modification layer. The amount of residual solder on the surface of Ni–W alloy-modified Cu-based microstructures after shearing of solder balls is less than that of Au/Ni–W-modified Cu-based microstructures, while the pure Cu-based microstructures have the most residual solder, as shown in Fig. 7(a) and (b), and Fig. 7(c). Obviously, the amount of residual solder on the fracture surface is directly proportional to the average shear strength of the soldering interface. A greater average shear strength of the soldering interface results in a larger
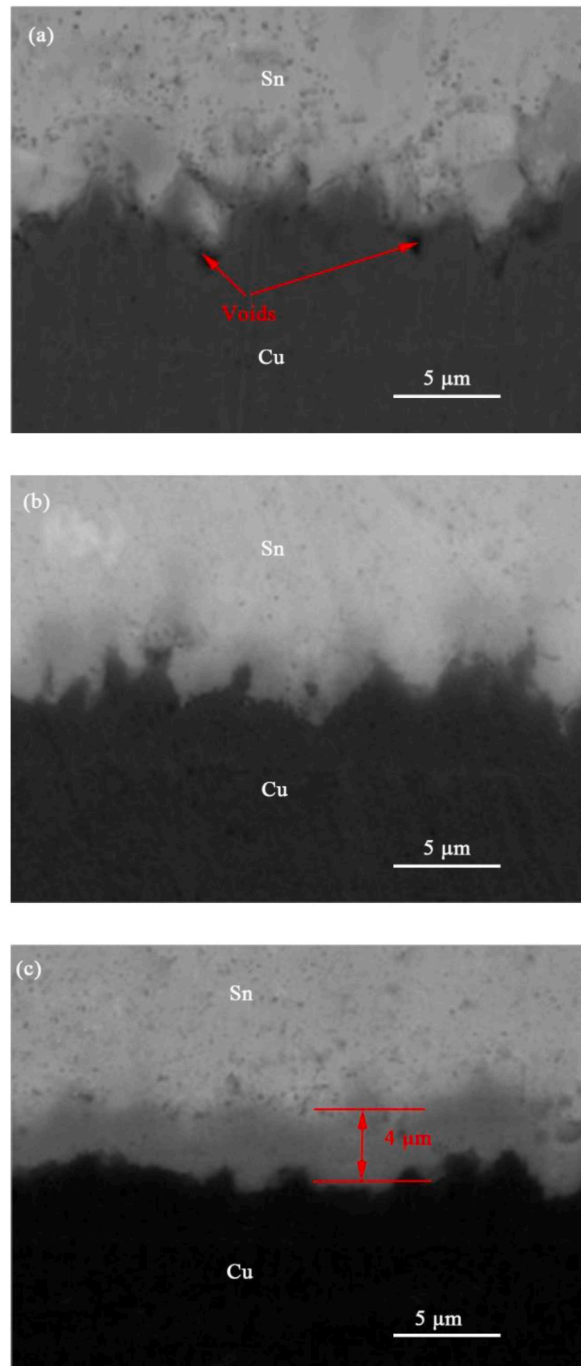


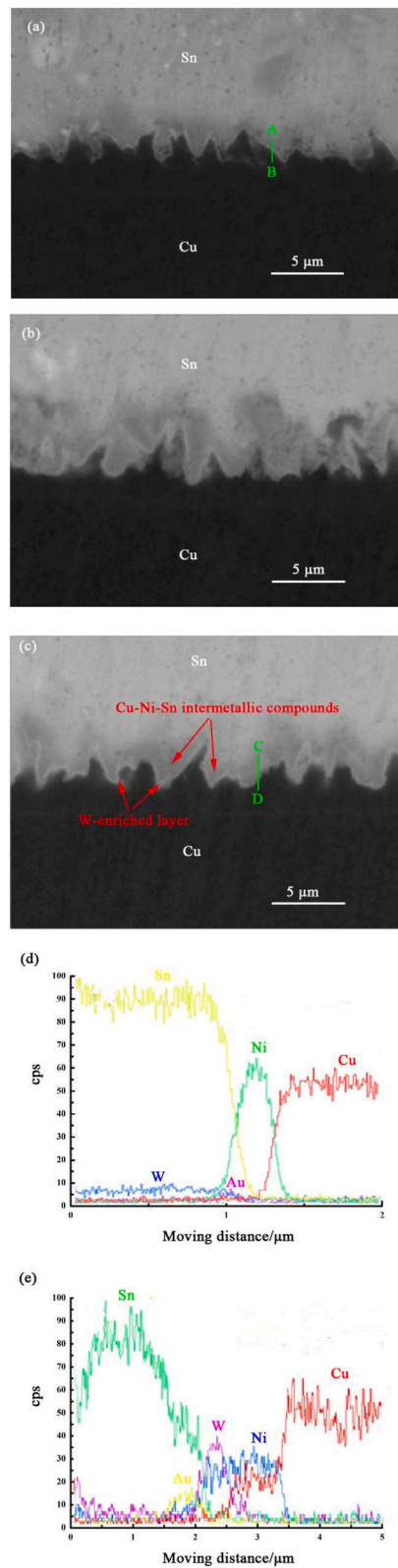**Fig. 8.** SEM image of the diffusion couple interface of Sn/pure Cu-based micro-nano hierarchical structure: (a) aging for 10 min (b) aging for 30 min (c) aging for 60 min.
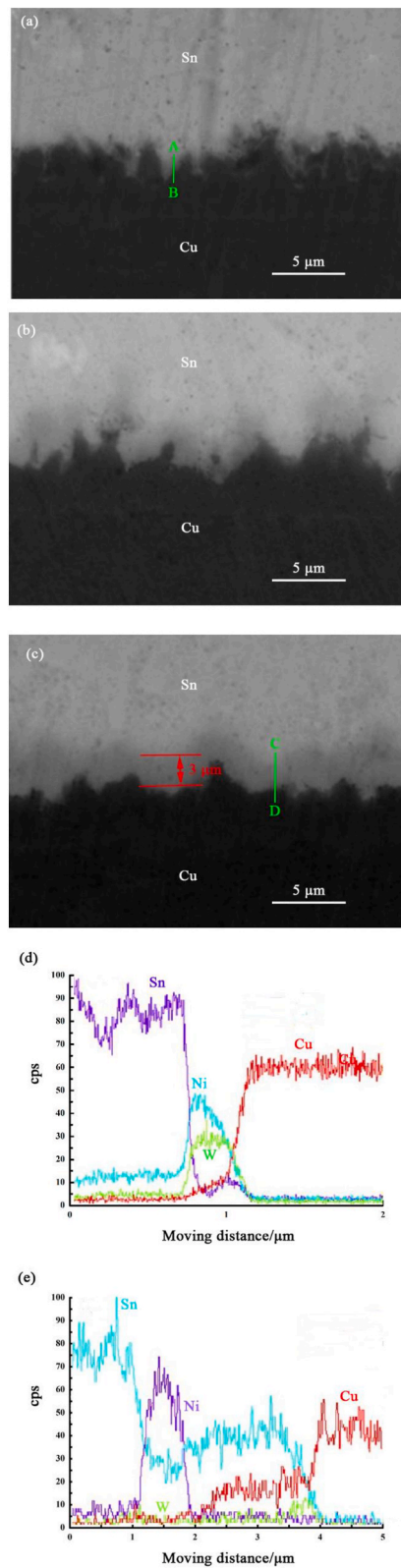
**Fig. 9.** SEM image of diffusion couple interface of Sn/Ni–W alloy modified Cu-based micro-nano hierarchical structure: (a) aging for 10 min (b) aging for 30 min (c) aging for 60 min (d) AB line scanning results (e) CD line scanning results.

**Fig. 10.** SEM images of diffusion couple interfaces of Sn/Au/Ni–W alloy-modified Cu-based micro-nano hierarchical structures: (a) aging for 10 min (b) aging for 30 min (c) aging for 60 min (d) AB line scanning results (e) CD line scanning results.

quantity of solder left on the copper structure at the fracture surface. Judging from the fracture surfaces demonstrated in Fig. 7(c), the fracture surfaces of the Au/Ni–W-modified Cu-based microstructures basically occur inside the solder ball matrix, which is a pure toughness fracture.

### 3.4. Micromorphology of soldering interface after aging treatment

The samples obtained by soldering different modified layers of copper-based microstructures with SAC305 solder were aged at 180 °C under the conditions of soldering pressure of 10000 gf (20 MPa), soldering time of 3 s, and ultrasonic vibration of 3 s. The samples were then aged at 180 °C. Fig. 8(a) and (b), and Fig. 8(c) show the SEM image of the interfacial diffusion couple between the pure copper-based microstructures and tin solder. It is found that with the increase of aging time, the interface between the pure copper-based microstructure and the tin solder increases gradually forming a diffusion layer. The copper-based micro-nano-graded structure gradually disappears, and the gap at the soldering interface disappears due to atomic interdiffusion filling. After aging for 60 min, the thickness of the Cu–Sn IMC formed at the soldering interface is about 4 μm.

Fig. 9(a) and (b), and Fig. 9(c) show the SEM image of the diffusion couple at the interface between the Ni–W alloy modified Cu-based microstructure and tin solder. It is found that the interface between the Ni–W alloy-modified Cu-based microstructures and tin solder is still visible after aging for 30 min with the micro-nano-graded structure. And the micro-nano-graded structure disappeared after aging for 60 min, and IMCs with a thickness of about 3 μm were generated by reaction with tin. Fig. 9 (d) and Fig. 9 (e) show the results of the elemental line scanning patterns at lines AB and CD in Fig. 9(a) and (c), respectively. It can be found that the Sn element erodes deeper into the copper substrate with the aging treatment time.

The W atoms in the Ni–W alloy are refractory atoms, producing a similar "pinning" effect. The presence of W atoms hinders the diffusion between Cu and Sn atoms. The Ni–W alloy coating in this paper has an amorphous structure with a W content of 60 %. Since the atomic radius of W is larger than that of Ni, the solid solution of W atoms causes distortion of the Ni lattice. This causes the free energy of the system to increase, the diffusion activation energy of the atoms also increases, and the atomic diffusion capacity decreases. On the other hand, as the atomic diffusion concentration gradient at the soldering is decreasing, the energy provided is reduced. Atomic diffusion capacity decreases. This creates a blocking effect to some extent.

Fig. 10(a) and (b), and Fig. 10(c) show the SEM image of the interfacial diffusion couple between Au/Ni–W alloy-modified Cu-based microstructure and tin solder. The interfacial diffusion reaction between Au/Ni–W-modified Cu-based microstructure and tin solder is much slower, and there is a "bright layer" structure at the interface, which is an enriched layer of W. The amorphous Ni–W alloy coating is subjected to high-temperature aging. The coating is composed of a mixture of IMCs such as $Ni_4W$ and NiW. W is a chemically stable metal and does not react with tin solder. $Ni_4W$ and NiW in the Ni–W alloy layer also do not react with Sn atoms, and only Ni atoms react with Sn atoms. Sn continuously consumes the Ni in the Ni–W alloy layer, making the W content in the alloy layer increase, and a new phase with brighter lining is generated at the interface between the Ni–W alloy layer and the soldered copper structure. On the other hand, the high temperature of the aging treatment provides energy for the nucleation and growth of IMCs in the "bright layer" structure and at the soldering interface, resulting in a continuous increase in the thickness of the atomic diffusion layer. However, after 30 min of aging, the thickness of the "bright layer" structure does not change with aging time and is about 100 nm because the activation energy of the "bright layer" is much higher than that of the other IMCs and it cannot continue to grow.

The interface between the Au/Ni–W modified Cu-based microstructures and the tin solder was aged at 180 °C for 60 min, and the diffusion couple interface is shown in Fig. 10(c). It is found that there exists a layer of "bright layer" structure with obvious lining degree at the whole diffusion interface, which is a W-enriched layer. Above the "bright layer" structure, a different lining from that of the enriched layer is observed, which should be due to the generation of a new phase, and combined with the previous analysis, it is a Cu–Ni–Sn IMC. On the other hand, the lining below the "bright layer" structure is uniform, and no new phase generation is found. It can be assumed that the W-rich "bright layer" structure can effectively prevent the downward diffusion of Sn atoms and the upward diffusion of Cu atoms, thus limiting the excessive growth of Cu–Sn IMCs. Fig. 10(d) and (e) show the results of elemental line scanning spectra at lines AB and CD in Fig. 10(a) and (c), respectively. It can be found that the Au plating at the soldering interface disappears with the extension of the aging treatment time, but there is still an aggregation of Au elements at the interface.

## 4. Conclusion

(1) Under the conditions of soldering pressure of 10000 gf (20 MPa), soldering time of 3 s, and ultrasonic vibration of 3 s, the thickness of 180 nm Ni–W alloy layer and the thickness of 5 nm Au film-modified Cu-based microstructures are embedded sufficiently in the soldering interface with the solder ball, and the soldering interface has a good bonding quality. The Au/Ni–W alloy modification layer can effectively improve the surface hardness of Cu-based microstructures, forming a larger hardness difference with tin solder and reducing the formation of holes.

(2) The average shear strength of Au/Ni–W modified Cu-based microstructure with solder is 43.06 MPa, which is comparable to that of reflow soldering. While the average shear strength of Ni–W alloy modified Cu-based microstructure with solder is only 23.4 MPa. The amorphous Ni–W alloy forms a dense oxide film during the ultrasonic process. Additional energy is consumed by the micro-nano-graded structures to puncture the oxide film, and the oxide film does not react with the solder ball, resulting in a decrease in the solder strength. The thin Au layer can prevent the oxidation of Ni–W alloy modification layer and reduce the oxidation problem in soldering.

(3) At the interface between the Au/Ni–W modified Cu-based microstructure and the tin solder, a W-enriched "bright layer" structure appears at the soldering interface after a long aging treatment at 180 °C. New phases are generated on the solder side

above the "bright layer", while no new phases appear on the side of the Cu-based micro-nano-graded structure below the "bright layer". The presence of the Ni–W alloy layer slows down the interdiffusion between Cu–Sn, blocks the growth of Cu–Sn IMCs, and reduces the reliability problems caused by interfacial failure. This room-temperature, solid-state, instantaneous soldering method is expected to find application in electronic packaging.

## Funding statement

## Data availability statement

Data will be made available on request.

## CRediT authorship contribution statement

**Jin Xiao:** Funding acquisition, Formal analysis, Conceptualization. **Qian Zhai:** Investigation. **Jia Luo:** Software.

## Declaration of competing interest

The authors declare that they have no known competing financial interests or personal relationships that could have appeared to influence the work reported in this paper.

## References

[1]  Y. Mou, J. Liu, H. Cheng, Y. Peng, M. Chen, Facile preparation of self-reducible Cu nanoparticle paste for low temperature Cu-Cu bonding, Jom 71 (2019) 3076–3083, https://doi.org/10.1007/s11837-019-03517-5.

[2]  T.-F. Lu, T.-Y. Lai, Y.Y. Chu, Y.S. Wu, Effect of nanotwin boundary on the Cu–Cu bonding, ECS Journal of Solid State Science and Technology 10 (7) (2021) 074001, https://doi.org/10.1149/2162-8777/ac0e14.

[3]  Y.-G. Lee, M. McInerney, Y.-C. Joo, I.-S. Choi, S.E. Kim, Copper bonding technology in heterogeneous integration, Electron. Mater. Lett. 20 (1) (2024) 1–25, https://doi.org/10.1007/s13391-023-00433-4.

[4]  Z.-J. Hong, M.-W. Weng, C.-H. Chen, M.-P. Hsu, H.-W. Hu, T.-Y. Lin, Y.-C. Hung, K.-N. Chen, Scheme for multi-chiplet integration with low thermal budget by asymmetric Cu-Cu bonding with Au passivation bonding structure, IEEE Electron. Device Lett. 44 (3) (2023) 492–495, https://doi.org/10.1109/LED.2023.3239011.

[5]  K. Ariga, Nanoarchitectonics: the method for everything in materials science, Bull. Chem. Soc. Jpn. 97 (1) (2024) uoad001, https://doi.org/10.1093/bulcsj/uoad001.

[6]  K.-C. Shie, P.-N. Hsu, Y.-J. Li, K.-N. Tu, C. Chen, Effect of bonding strength on electromigration failure in Cu–Cu bumps, Materials 14 (21) (2021) 6394, https://doi.org/10.3390/ma14216394.

[7]  Y. Cai, B. Xu, X. Ma, J. Haider, Y. Mao, S. Wang, Bonding of graphite to Cu with metal multi-foils, Arch. Civ. Mech. Eng. 23 (1) (2023) 58, https://doi.org/10.1007/s43452-023-00603-z.

[8]  J. Fan, T. Shi, Z. Tang, B. Gong, J. Li, J. Huang, T. Li, Low-temperature Cu-Cu bonding process based on the Sn-Cu multilayer and self-propagating reaction joining, J. Electron. Mater. 48 (2019) 1310–1317, https://doi.org/10.1007/s11664-018-6827-z.

[9]  Z.-J. Hu, X.-P. Qu, H. Lin, R.-D. Huang, X.-C. Ge, M. Li, S.-M. Chen, Y.-H. Zhao, Cu CMP process development and characterization of Cu dishing with 1.8 μm Cu pad and 3.6 μm pitch in Cu/SiO2 hybrid bonding, Jpn. J. Appl. Phys. 58 (SH) (2019) SHHC01, https://doi.org/10.7567/1347-4065/ab17c4.

[10]  L. Sun, M.-h. Chen, L. Zhang, P. He, L.-s. Xie, Recent progress in SLID bonding in novel 3D-IC technologies, J. Alloys Compd. 818 (2020) 152825, https://doi.org/10.1016/j.jallcom.2019.152825.

[11]  J.-J. Jhan, K. Wataya, H. Nishikawa, C.-M. Chen, Electrodeposition of nanocrystalline Cu for Cu-Cu direct bonding, J. Taiwan Inst. Chem. Eng. 132 (2022) 104127, https://doi.org/10.1016/j.jtice.2021.10.027.

[12]  S.L. Chua, J.M. Chan, S.C.K. Goh, C.S. Tan, Cu–Cu bonding in ambient environment by Ar/N 2 plasma surface activation and its characterization, IEEE Trans. Compon. Packag. Manuf. Technol. 9 (3) (2018) 596–605, https://doi.org/10.1109/TCPMT.2018.2875460.

[13]  Z. Wu, J. Cai, Q. Wang, J. Wang, Low temperature Cu-Cu bonding using copper nanoparticles fabricated by high pressure PVD, AIP Adv. 7 (3) (2017) 035306, https://doi.org/10.1063/1.4978490.

[14]  M. Lykova, I. Panchenko, U. Künzelmann, J. Reif, M. Geidel, M.J. Wolf, K.-D. Lang, Characterisation of Cu/Cu bonding using self-assembled monolayer, Solder. Surf. Mt. Technol. 30 (2) (2018) 106–111, https://doi.org/10.1108/SSMT-10-2017-0033.

[15]  D.F.O. Braga, R. Maciel, L. Bergmann, L.F.M. da Silva, V. Infante, J.F. dos Santos, P.M.G.P. Moreira, Fatigue performance of hybrid overlap friction stir welding and adhesive bonding of an Al-Mg-Cu alloy, Fatig. Fract. Eng. Mater. Struct. 42 (6) (2019) 1262–1270, https://doi.org/10.1111/ffe.12933.

[16]  J. Liang, Y. Ohno, Y. Yamashita, Y. Shimizu, S. Kanda, N. Kamiuchi, S. Kim, K. Koji, Y. Nagai, M. Kasu, Characterization of nanoscopic Cu/diamond interfaces prepared by surface-activated bonding: implications for thermal management, ACS Appl. Nano Mater. 3 (3) (2020) 2455–2462, https://doi.org/10.1021/acsanm.9b02558.

[17]  J. Li, Y. Zhang, H. Zhang, Z. Chen, C. Zhou, X. Liu, W. Zhu, The thermal cycling reliability of copper pillar solder bump in flip chip via thermal compression bonding, Microelectron. Reliab. 104 (2020) 113543, https://doi.org/10.1016/j.microrel.2019.113543.

[18]  K.D. Min, K.-H. Jung, C.-J. Lee, B.-U. Hwang, S.-B. Jung, Enhancement of electrochemical and thermal bonding reliability by forming a Cu3Sn IMC using Cu and Sn–58Bi, J. Alloys Compd. 857 (2021) 157595, https://doi.org/10.1016/j.jallcom.2020.157595.

[19]  D. Ishikawa, B.N. An, M. Mail, H. Wurst, B. Leyrer, T. Blank, M. Weber, S. Ueda, H. Nakako, Y. Kawana, Bonding strength of Cu sinter die-bonding paste on Ni, Cu, Ag, and Au surfaces under pressureless bonding process, Transactions of The Japan Institute of Electronics Packaging 13 (2020) E19, https://doi.org/10.5104/jiepeng.13.E19-017-1. E1017-1-E19-017-11.

[20]  B. Park, M. Saito, J. Mizuno, H. Nishikawa, Robust shear strength of Cu–Au joint on Au surface-finished Cu disks by solid-state nanoporous Cu bonding, Microelectron. Eng. 260 (2022) 111807, https://doi.org/10.1016/j.mee.2022.111807.

[21]  J. Wang, X. Liu, F. Huo, K. Kariya, N. Masago, H. Nishikawa, Novel transient liquid phase bonding method using In-coated Cu sheet for high-temperature die attach, Mater. Res. Bull. 149 (2022) 111713, https://doi.org/10.1016/j.materresbull.2021.111713.

[22]  J.H. Lau, State of the art of lead-free solder joint reliability, J. Electron. Packag. 143 (2) (2020), https://doi.org/10.1115/1.4048037.

[23]  J. Wang, S. Xue, P. Zhang, P. Zhai, Y. Tao, The reliability of lead-free solder joint subjected to special environment: a review, J. Mater. Sci. Mater. Electron. 30 (10) (2019) 9065–9086, https://doi.org/10.1007/s10854-019-01333-w.

[24] K.-K. Xu, L. Zhang, L.-L. Gao, N. Jiang, L. Zhang, S.-J. Zhong, Review of microstructure and properties of low temperature lead-free solder in electronic packaging, Sci. Technol. Adv. Mater. 21 (1) (2020) 689–711, https://doi.org/10.1080/14686996.2020.1824255.

[25] J. Xiao, W. Cheng, Q. Fu-kang, Interfacial reaction of Sn-1.5 Ag-2.0 Zn low-silver lead-free solder with oriented copper, Heliyon 10 (2024) e27010, https://doi.org/10.1016/j.heliyon.2024.e27010.

[26] M.-y. Xiong, L. Zhang, Interface reaction and IMC growth behavior of Sn-Ag-Cu lead-free solder joints on different substrates in electronic packaging, J. Mater. Sci. 54 (2) (2019) 1741–1768, https://doi.org/10.1007/s10853-018-2907-y.

[27] Z. Yang, L. Li, W. Chen, X. Jiang, Y. Liu, Numerical and experimental study on laser soldering process of SnAgCu lead-free solder, Mater. Chem. Phys. 273 (2021) 125046, https://doi.org/10.1016/j.matchemphys.2021.125046.

[28] H. Qiu, X. Hu, S. Li, Y. Wan, Q. Li, Shear strength and fracture surface analysis of lead-free solder joints with high fraction of IMCs, Vacuum 180 (2020) 109611, https://doi.org/10.1016/j.vacuum.2020.109611.

[29] S. Li, X. Wang, Z. Liu, F. Mao, Y. Jiu, J. Luo, L. Shangguan, X. Jin, G. Wu, S. Zhang, P. He, W. Long, Research status of evolution of microstructure and properties of Sn-based lead-free composite solder alloys, J. Nanomater. 2020 (2020) 8843166, https://doi.org/10.1155/2020/8843166.

[30] D. Qu, C. Li, L. Bao, Z. Kong, Y. Duan, Structural, electronic, and elastic properties of orthorhombic, hexagonal, and cubic Cu3Sn IMCs in Sn–Cu lead-free solder, J. Phys. Chem. Solid. 138 (2020) 109253, https://doi.org/10.1016/j.jpcs.2019.109253.

[31] D.L. Han, Y.-A. Shen, S. He, H. Nishikawa, Effect of Cu addition on the microstructure and mechanical properties of In–Sn-based low-temperature alloy, Mater. Sci. Eng., A 804 (2021) 140785, https://doi.org/10.1016/j.msea.2021.140785.

[32] X. Li, J. Wang, M. Li, W. Hou, Low-temperature, short-time, wafer-level bonding for Cu/Sn/Cu solid-state-diffusion interconnect in 3-D integration, Phys. Scripta 98 (2) (2023) 025608, https://doi.org/10.1088/1402-4896/acab8c.

[33] H. Wang, W.S. Leong, F. Hu, L. Ju, C. Su, Y. Guo, J. Li, M. Li, A. Hu, J. Kong, Low-temperature copper bonding strategy with graphene interlayer, ACS Nano 12 (3) (2018) 2395–2402, https://doi.org/10.1021/acsnano.7b07739.

[34] M.-l. Li, L. Zhang, L.-l. Gao, X. Wang, C. Chen, X. Lu, Interfacial structures and mechanical properties of Cu/Sn/Cu containing SiC nanowires under transient liquid phase bonding, Intermetallics 148 (2022) 107641, https://doi.org/10.1016/j.intermet.2022.107641.

[35] Y. Sun, J. Wang, X. Zhang, C. Yang, A. Hu, T. Hang, Y. Wu, H. Ling, M. Li, Low-temperature insertion bonding using electroless Cu-Co-P micro-cones array with controllable morphology, Electron. Mater. Lett. 17 (6) (2021) 459–470, https://doi.org/10.1007/s13391-021-00302-y.